Supplementary Materials for

Restoring universality to the pinch-off of a bubble

Amir A. Pahlavan,[1,2] Howard A. Stone,[2] Gareth H. McKinley,[1] and Ruben Juanes[1]

[1]*Massachusetts Institute of Technology, Cambridge, Massachusetts, USA*

[2]*Department of Mechanical and Aerospace Engineering,*

Princeton University, Princeton, New Jersey, USA[*]

(Dated:)

[*] pahlavan@princeton.edu

www.pnas.org/cgi/doi/10.1073/pnas.1819744116

This PDF file includes:

1. Materials and Methods

2. Supplementary Text

3. Figs. S1 and S2

4. Captions for Movies S1 and S2

I. MATERIALS AND METHODS

We use precision-made borosilicate glass capillary tubes with two different inner diameters ($d = 280, 750$ μm). We wash the capillary tubes with isopropyl alcohol and ethanol, followed by an ultrasonic cleaning step in a de-ionized water bath for one hour. The capillary tubes are then dried using compressed nitrogen gas. We use glycerol (viscosity $\mu = 1.4$ Pa.s) and 90% glycerol-water mixture (viscosity $\mu = 0.2$ Pa.s) as the liquid phase. Both liquids are partially wetting to the tube with a contact angle of ≈ 25 degrees. The receding contact line speed is proportional to the equilibrium contact angle cubed ($\sim \theta_{eq}^3$) [1, 2]; therefore, to accelerate the pinch-off process, we make the tubes less wetting to the liquid through heat-assisted chemical vapor deposition step of trichloro(1H,1H,2H,2H-perfluorooctyl)silane (Sigma-Aldrich, USA) in a vacuum oven, which leads to a contact angle of $\approx 65^\circ$.

The capillary tube is open to the atmosphere at the left end and is connected to a syringe pump at the right end. The tube is initially filled with glycerol and then the glycerol is withdrawn at a specified flow rate Q from the right end of the tube using a syringe pump (CETONI low pressure pump neMESYS), leading to the air penetrating the tube from the left side. To achieve refractive-index matching and an undistorted view of the displacement process, we house the circular capillary tube inside a square tube (both tubes are made of borosilicate glass) and fill the gap between the two with glycerol. When the capillary tube is filled with glycerol, light goes through the system without any refraction (white color in Fig. 1 of the main text). When air penetrates the tube, it leads to the refraction of light to the center of the tube; therefore air appears in black color with a straight white line in the middle. The capillary tube is backlit with a LED light source (120E, Veritas). Imaging is done from the front side using a high-speed camera (Phantom Micro 320) at a typical frame-rate of 10–25 kfps. A 4X lens is mounted on the camera leading to a resolution of 1.7 μm/pixel.

II. LONG-WAVE MODEL FOR THE DEWETTING RIM

When glycerol is withdrawn from the tube at a high-enough flow rate ($Q > Q_c$) [2], air penetrates the tube from the left side leaving a film of the liquid on the walls. Since the liquid is partially wetting to the tube ($\theta_{eq} \approx 65^\circ$) it starts dewetting from the tube wall, forming a growing dewetting rim (Fig. 1). Initially, the flow in the film is mainly due to the receding of the contact line, leading to the flow to be mainly parallel to the tube axis. This observation allows us to describe the dynamics of the growing dewetting rim using a long-wave approximation [2]:

$$\frac{\partial \tilde{r}}{\partial \tilde{\tau}} = \frac{1}{(16)^2}\frac{1}{\tilde{r}}\frac{\partial}{\partial \tilde{z}}\left(\mathcal{M}(\tilde{r})\frac{\partial}{\partial \tilde{z}}\Big[\Pi(\tilde{r}) - \tilde{\kappa}\Big]\right), \tag{1}$$

where $\tilde{r}(\tilde{z},\tilde{\tau})$ is the radius of bubble neck, $\mathcal{M}(\tilde{r}) = 1 - 16\tilde{r}^2 + 48\tilde{r}^4 - 64\tilde{r}^4\ln 2\tilde{r}$ is the mobility, $\Pi(\tilde{r}) = 6(1-\cos\theta_{eq})(\delta^2/(1/2-\tilde{r})^3)(1-\delta/(1/2-\tilde{r}))$ is the disjoining pressure with δ as the precursor film thickness, and $\tilde{\kappa} = 1/\tilde{r} - \tilde{r}_{\tilde{z}\tilde{z}}$ is the curvature. Here, all length scales are non-dimensionalized by the tube diameter d, and the dimensionless time to the pinch-off is defined as $\tilde{\tau} = \tau/t^*$, where $\tau = (t_0 - t)$ is the time to the pinch-off with t_0 as the breakup time and $t^* = \mu d/\gamma$ is the visco-capillary time scale.

Near the point of pinch-off, we postulate that the shape of the profile becomes self-similar: $\tilde{R}(\xi) = \tilde{r}(\tilde{z},\tilde{\tau})/\tilde{\tau}^\alpha$, and $\xi = (\tilde{z} - \tilde{z}_0)/\tilde{\tau}^\beta$. We can neglect the disjoining pressure in the vicinity of the singularity, which is far away from the contact line. Substituting this ansatz back into Eq. (1), we recover Eq. (1) of the main text:

$$(-\alpha\tilde{R} + \beta\xi\tilde{R}')\tilde{\tau}^{\alpha-1} = \frac{1}{(16)^2}\frac{1}{\tilde{R}}\left(\left[-\frac{2}{\tilde{R}^3}\tilde{R}'^2 + \frac{1}{\tilde{R}^2}\tilde{R}''\right]\tilde{\tau}^{-2(\alpha+\beta)} + \tilde{R}''''\tilde{\tau}^{-4\beta}\right), \tag{2}$$

where prime indicates differentiation. For all the terms to balance in time we need to have $\alpha = \beta = 1/5$, which leads to $\tilde{R}(\xi) = \tilde{r}(\tilde{z},\tilde{\tau})/\tilde{\tau}^{1/5}$, and $\xi = (\tilde{z} - \tilde{z}_0)/\tilde{\tau}^{1/5}$. The equation governing the dewetting rim in the early self-similar regime is therefore the following:

$$(-\tilde{R} + \xi\tilde{R}') = \frac{5}{(16)^2}\frac{1}{\tilde{R}}\left(\left[-\frac{2}{\tilde{R}^3}\tilde{R}'^2 + \frac{1}{\tilde{R}^2}\tilde{R}''\right] + \tilde{R}''''\right), \tag{3}$$

which represents the balance of viscous forces on the left-hand side with the surface tension forces on the right-hand side.

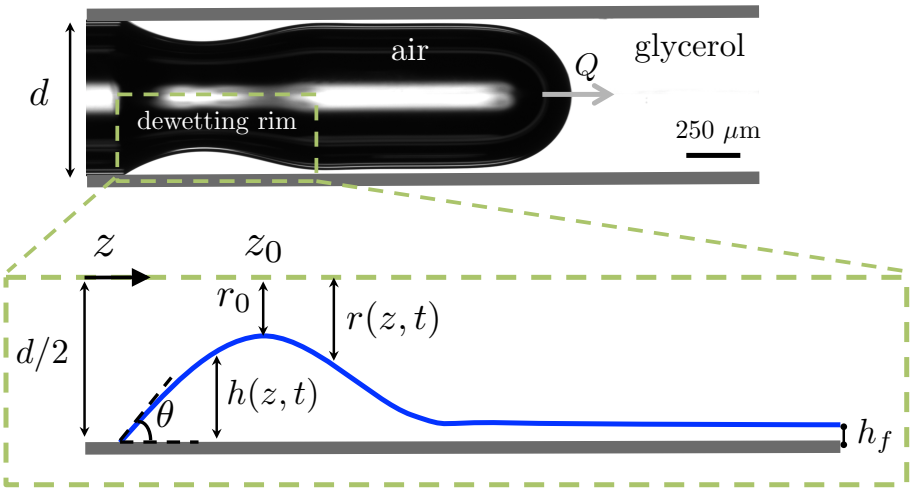

FIG. 1. Schematics of the dewetting rim: as the contact line recedes from the tube wall, liquid accumulates behind it and the rim keeps growing. The dynamics of this growing rim can be described using a long-wave approximation (Eq. (1)). The film thickness downstream of the rim is set by the Taylor–Bretherton scaling $h_f/(d/2) = 1.34\mathrm{Ca}_f^{2/3}/(1+1.34\times 2.5\mathrm{Ca}_f^{2/3})$, where $\mathrm{Ca}_f = \mu U_f/\gamma$ with U_f as the air finger velocity[3–6]. This relationship combined with the conservation of mass: $Q = \pi(d/2 - h_f)^2 U_f$ determine both the finger velocity and the film thickness.

This type of ordinary differential equations typically leads to an infinite family of solutions, where only one is found to be stable [7, 8]. To obtain the self-similar solution of the ODE, we solve the original partial differential equation (1) numerically and extract the self-similar solution from the late-time solution of the PDE very close to the point of pinch-off. The self-similar solution obtained using this technique is shown as the dashed line in Fig. 3(b) of the main text, and shows an excellent agreement with the experimental data at the early-time self-similar regime, where the long-wave model is valid.

III. CROSSOVER TIME

To estimate the crossover time between the two regimes, we compare their corresponding radial velocities. In the early-time regime, the growth rate of the dewetting rim is proportional to the velocity of the receding contact line, i.e. $dr_0/d\tau \sim u_{cl} \sim (\gamma/\mu)\theta_{eq}^3$, which is nearly constant for a given wettability [1, 2]. In the late-time regime, the bubble neck close to the point of singularity can be approximated as an axisymmetric cylinder, and the flow in the viscous fluid can be approximated as radial. The normal viscous stress generated by the radial flow is balanced by surface tension, leading to $dr_0/dt = -\gamma/(2\mu)(1 - 2r_0/r_c)$ [9], where $r_c \approx r_c(t = 0))$ is the axial radius of curvature. The radius of the neck can therefore be approximated as $r_0(t) = r_{00}[1 - r_c/(2r_{00})]e^{\gamma t/(\mu r_c)} + r_c/(2r_{00})$ where $r_{00} = r_0(t = 0)$, leading to $dr_0/d\tau \sim (\gamma/\mu)e^{-\tau/t^*}$ as the radial velocity in the late-time regime [9]. Note that very close to the point of pinch-off, we have $r_0 \ll r_c$, leading to $dr_0/d\tau = \gamma/(2\mu)$, which is the familiar linear scaling in time [10]. Equating the two radial velocities corresponding to the early and late-time regimes we obtain an estimate of the crossover time $\tau_c \sim t^* = \mu d/\gamma$, indicating that the visco-capillary time scale sets the point of transition between the two regimes.

IV. SELF-SIMILARITY OF THE BUBBLE NECK IN A LARGE QUIESCENT TANK

Here, we briefly review how to determine the value of the exponent β in the second self-similar regime [11]. In the late-time self-similar regime, we can approximate the bubble neck as a cylinder, which effectively acts as a sink sucking the liquid radially towards the tube center. The normal viscous stress jump across the air-liquid cylindrical interface is balanced by the surface tension, leading to $\partial r/\partial t = -\gamma/(2\mu)$. Therefore, the neck profile is simply translated in time without changing its shape. We postulate the neck profile becomes self-similar, following a scaling ansatz $\tilde{R}(\xi) = \tilde{r}(\tilde{z}, \tilde{\tau})/\tilde{\tau}^{\alpha}$, and $\xi = (\tilde{z} - \tilde{z}_0)/\tilde{\tau}^{\beta}$. Substituting this ansatz back into the governing equation for the neck profile, we obtain:

$$-\alpha\tilde{\tau}^{\alpha-1}\tilde{R} + \beta\tilde{\tau}^{\alpha-1}\xi\tilde{R}' = -1, \tag{4}$$

where prime indicates differentiation. For all the terms to balance in time we need to have $\alpha = 1$. The value of the exponent β, however, cannot be determined from dimensional analysis, indicating that the self-similarity is of the second kind [12].

The solution of Eq. (4) is described by $\tilde{R} = 1 + a\tilde{\xi}^{1/\beta}$, in which a is a constant of integration that depends on the outer solution away from the singularity. Close to the pinch-off time, the neck profile away from the singularity becomes effectively frozen in time, which leads to a constraint on the behavior of the self-similar solution: $\tilde{r}(\tilde{z} \to \tilde{z}_0 \pm \epsilon, \tilde{\tau} \to \epsilon) = \tilde{\tau}^{\alpha}\tilde{R}((\tilde{z} - \tilde{z}_0)/\tilde{\tau}^{\beta}) = \text{const}$, and therefore we need to have $\tilde{R}(\xi \to \pm\infty) \sim \xi^{\alpha/\beta}$. The regularity condition also implies that $1/\beta$ must be a positive even integer, and $a > 0$. We can therefore have a discrete family of solutions for β, i.e. $\beta_i = 1/(2i)$ with $i = 1, 2, ...$ This is similar to the breakup of a drop, where also an infinite family of solutions is obtained [7, 8].

To find out which one of these solutions is selected, we need to address the stability of these solutions. Briefly, we use a change of variables $T = -\ln\tilde{\tau}$, rewriting the equation governing the self-similar profile as $R_T = R - \beta\xi R' - 1$, which is a dynamical system representation of the original equation, for which the original self-similar solution will be a fixed point. We can therefore perturb the self-similar solution as $\tilde{R}(\xi, T) = \bar{R}(\xi) + \epsilon e^{nT}P(\xi)$, where n is the eigenvalue and P is the eigenfunction. The stability analysis [11] shows that the stable solution is

described by $\beta = 1/2$, i.e. $\tilde{R}(\xi) = 1 + a\xi^2$. This implies that the neck profile can be described as $\tilde{r}(\tilde{z}, \tilde{\tau}) = \tilde{\tau}(1 + a[(\tilde{z} - \tilde{z_0})/\tilde{\tau}^{1/2}]^2) = \tilde{\tau} + a(\tilde{z} - \tilde{z_0})^2$, which is a parabola that is simply translated in time.

V. EVOLUTION OF THE LATERAL LENGTH SCALE IN TIME

In Fig. 3 of the main text, we showed that using the lateral length scale $\zeta = \sqrt{r_0 r_c}$ extracted from the experimental data ($d = 750$ μm, $\mu = 1.4$ Pa.s, and Ca $= 0.008$), we can collapse the neck profiles during its entire time evolution onto a single parabola. To extract the axial length scale ζ, we fit a parabola to the neck profile in the vicinity of the minimum neck radius. Another technique recently developed by Wagoner et al. [13] extracts the axial length scale of the neck from the calculation of the pinch-off zone volume. The pinch-off zone is defined as the region between the minimum neck radius, r_0, and $r = \alpha r_0$ with $1 < \alpha < 2$. Fig. 2 shows that the neck volume at early times follows the scaling $\tilde{\tau}^{3/5}$ and at late times follows the scaling $\tilde{\tau}^{5/2}$. The neck volume scales as $r_0^2\zeta$, and we know that $\tilde{r}_0 \sim \tilde{\tau}^{1/5}$ at early times and $\tilde{r}_0 \sim \tilde{\tau}$ at late times. Therefore, the evolution of the neck volume in time indicates that $\tilde{\zeta} \sim \tilde{\tau}^{1/5}$ at early times and $\tilde{\zeta} \sim \tilde{\tau}^{1/2}$ at late times. Therefore, calculating the axial length scale using the new technique further confirms our results.

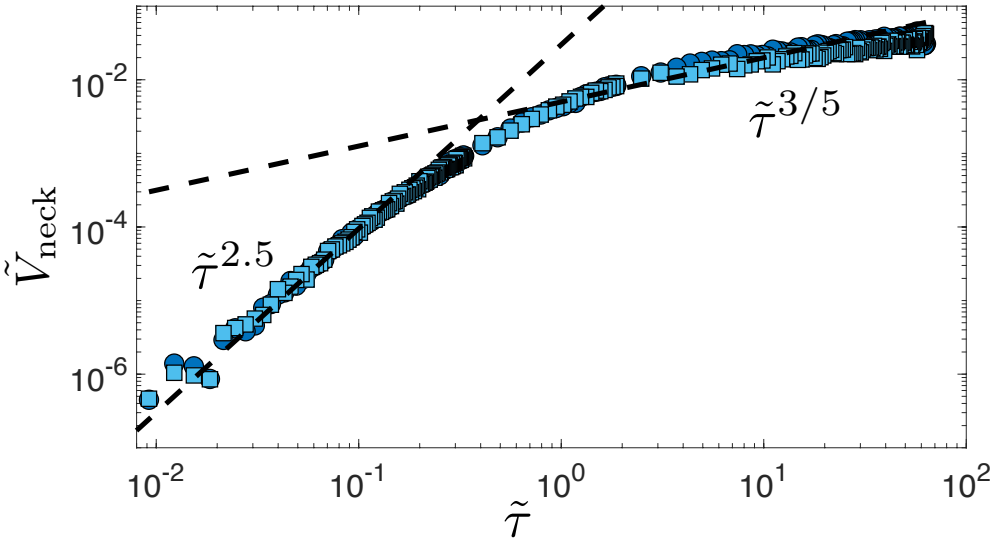

FIG. 2. The evolution of the volume of the pinching zone as a function of time to the pinch off, showing two distinct scalings in time at early and late time regimes. The squares and circles represent the neck half volume to the left and right of the minimum neck radius. Here, we have taken the pinch-off zone to be the region between the minimum neck radius, r_0, and $r = \alpha r_0$ with $\alpha = 1.3$. We have further confirmed that the scalings are insensitive to the value of α by repeating this procedure in the range $1.1 < \alpha < 1.7$.

In Fig. 3 we present the lateral length scale evolution data corresponding to all the 12 experiments. We find that, indeed, scaling the lateral length scale with the tube diameter and the time scale with the visco-capillary time collapses the data corresponding to all the experiments. The scaling of $\tilde{\zeta} = \sqrt{\tilde{r}_c \tilde{r}_0} \sim \tilde{\tau}^{1/2}$ in the late-time regime indicates that the axial radius of curvature in the second regime becomes time-independent. The asymptotic value of the axial curvature is therefore set by the first self-similar regime at the point of crossover between the two regimes, where $\tilde{\zeta} \approx 0.13$, leading to $\tilde{r}_{cf} \equiv \tilde{r}_c(\tilde{\tau} \to 0) \approx 0.07$, making this asymptotic curvature universal, in contrast to the non-universal case of bubble breakup in an unbounded reservoir [10].

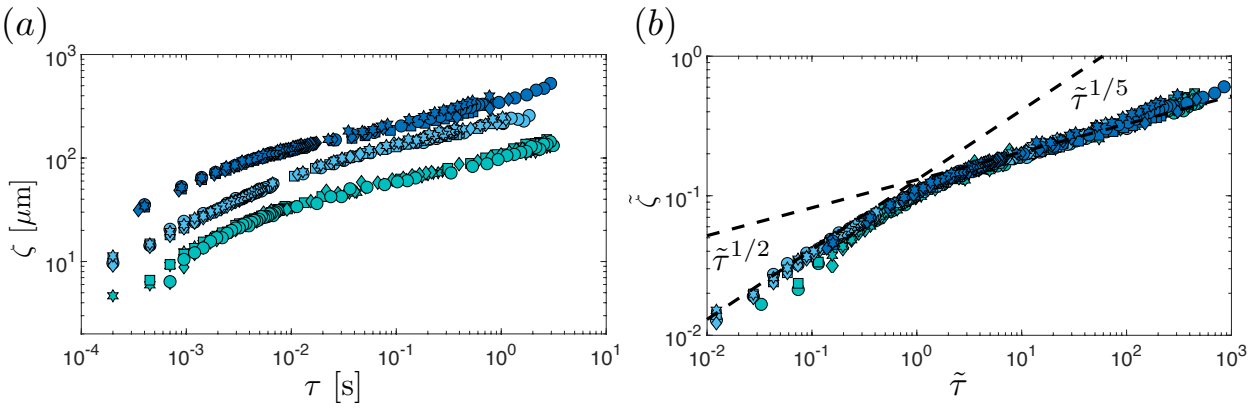

FIG. 3. The evolution of the lateral length scale of the bubble neck ($\zeta = \sqrt{r_0 r_c}$) in time: (a) dimensional, and (b) non-dimensional. Data from 12 different experiments are shown: light blue symbols correspond to $d = 750$ μm and $\mu = 1.4$ Pa.s; the cyan symbols correspond to $d = 280$ μm and $\mu = 1.4$ Pa.s; the dark blue symbols correspond to $d = 750$ μm and $\mu = 0.2$ Pa.s. Each color represents data corresponding to 4 different flow rates with Ca $= \mu U/\gamma \in [0.008, 0.02]$, where $U = 4Q/(\pi d^2)$ and Q is the liquid flow rate. While changing the flow rate does not influence the evolution of the lateral length scale ($\tilde{\zeta}$), changing μ or d shifts the curves.

VI. CAPTIONS OF SUPPLEMENTARY MOVIES

- **Movie S1**: Evolution of the dewetting rim and the ultimate breakup of the bubble in a capillary tube with the diameter $d = 280$ μm, and Ca $= 0.016$. The imaging is done at 20 kfps.

- **Movie S2**: Motion of a microbubble in the vicinity of the bubble neck. The microbubble here acts as a tracer, showing the flow direction, which is axially-dominant at early times and crosses over to a radially-dominant flow at late times.

[1] J. H. Snoeijer and J. Eggers. Asymptotic analysis of the dewetting rim. *Phys. Rev. E*, 82:056314, 2010.

[2] B. Zhao, A. A. Pahlavan, L. Cueto-Felgueroso, and R. Juanes. Forced wetting transition and bubble pinch-off in a capillary tube. *Phys. Rev. Lett.*, 120:084501, 2018.

[3] G. I. Taylor. Deposition of a viscous fluid on the wall of a tube. *Journal of Fluid Mechanics*, 10(2):161–165, 1961.

[4] F. P. Bretherton. The motion of long bubbles in tubes. *Journal of Fluid Mechanics*, 10(2):166–188, 1961.

[5] P. Aussillous and D. Quéré. Quick deposition of a fluid on the wall of a tube. *Physics of Fluids*, 12(10):2367–2371, 2000.

[6] E. Klaseboer, R. Gupta, and R. Manica. An extended bretherton model for long taylor bubbles at moderate capillary numbers. *Physics of Fluids*, 26(3):032107, 2014.

[7] D. T. Papageorgiou. On the breakup of viscous liquid threads. *Physics of Fluids*, 7(7):1529–1544, 1995.

[8] M. P. Brenner, J. R. Lister, and H. A. Stone. Pinching threads, singularities and the number 0.0304... *Physics of Fluids*, 8(11):2827–2836, 1996.

[9] R. Bolaños-Jiménez, A. Sevilla, C. Martínez-Bazán, D. van der Meer, and J. M. Gordillo. The effect of liquid viscosity on bubble pinch-off. *Physics of Fluids*, 21(7):072103, 2009.

[10] P. Doshi, I. Cohen, W. W. Zhang, M. Siegel, P. Howell, O. A. Basaran, and S. R. Nagel. Persistence of memory in drop breakup: The breakdown of universality. *Science*, 302(5648):1185–1188, 2003.

[11] J. Eggers. *Singularities at Interfaces*, volume 98 of *Lecture Notes of the Les Houches Summer School*, pages 101–132. Oxford University Press, 2012.

[12] G. I. Barenblatt. *Scaling, Self-similarity, and Intermediate Asymptotics: Dimensional Analysis and Intermediate Asymptotics*. Cambridge University Press, 1996.

[13] B. W. Wagoner, S. S. Thete, and O. A. Basaran. A new experimental method based on volume measurement for determining axial scaling during breakup of drops and liquid threads. *Physics of Fluids*, 30(8):082102, 2018.